journal

J. Am. Ceram. Soc., 95 [1] 338–349 (2012)
DOI: 10.1111/j.1551-2916.2011.04927.x

Modeling Oxidation Kinetics of SiC-Containing Refractory Diborides

T. A. Parthasarathy,[‡,§,†] R. A. Rapp,[¶] M. Opeka,[‖] and M. K. Cinibulk[‡]

[‡]Air Force Research Laboratory, Materials and Manufacturing Directorate, Wright-Patterson AFB, Ohio 45433-7817

[§]UES, Inc., Dayton, Ohio 45432

[¶]The Ohio State University, Columbus, Ohio 43235

[‖]Naval Surface Warfare Center, Carderock, Maryland 20817

Experimental data on the oxidation kinetics of SiC-containing diborides of Zr and Hf in the temperature regime of 1473–2273 K are interpreted using a mechanistic model. The model encompasses counter-current gas diffusion in the internal SiC depleted zone, oxygen permeation through borosilicate glass channels in the oxide scale, and boundary layer evaporation at the surface. The model uses available viscosity, thermodynamic and kinetic data for boria, silica, and borosilicate glasses, and a logarithmic mean approximation for compositional variations. The internal depletion region of SiC is modeled with CO/CO_2 counter diffusion as the oxygen transport mechanism. Data reported for pure SiC in air/oxygen, for ZrB_2 containing varying volume fractions of SiC, and for SiC–HfB_2 ultra-high temperature ceramics (UHTCs) by different investigations were compared with quantitative predictions of the model. The model is found to provide good correspondence with laboratory-furnace-based experimental data for weight gain, scale thicknesses, and depletion layer thicknesses. Experimental data obtained from arc-jet tests at high enthalpies are found to fall well outside the model predictions, whereas lower enthalpy data were closer to model predictions, suggesting a transition in mechanism in the arc-jet environment.

I. Introduction

Refractory diborides, especially ZrB_2 and HfB_2, with SiC additions are being studied with great interest because of their high thermal conductivity, high melting point, and moderate resistance to environmental degradation in air at very high temperatures.[1–3] This combination of properties of these two-phase composites makes them promising for use in hypersonic vehicles as leading edge components, which are subject to high heat fluxes.[1] Several additions and compositional refinements are being tried to enhance their oxidation resistance, but SiC-containing ZrB_2 or HfB_2 are the most studied, with sufficient data to enable a modeling-based analysis and understanding of their oxidation behavior.[4–19]

A brief summary of experimental observations is as follows.[4–19] The oxidation behavior is dominated by parabolic kinetics despite formation of a porous oxide of the refractory metal. This protective behavior is attributed to the borosilicate glass that fills the pores of the porous oxide scale and often also results in a glassy external layer, as seen from Fig 1(a) (courtesy Prof. E Opila, University of Virgina). In a furnace under static air, a continuous external glassy layer is formed, but at high temperatures, it begins to flow due to a decrease in viscosity giving rise to some scatter in experimental data. The underlying porous oxide is almost always filled with the borosilicate glass. Underneath this oxide layer, some investigations have reported a depleted region where SiC is absent but the diboride is still intact as, for example, seen in Fig. 1(a). The depleted region is absent at low temperatures, but has been reported in samples exposed to high-temperature air. However, there is an inconsistency in the reported data with some studies not finding any depleted layers under the same conditions where others have observed them.[7,10,14,20,21] In some work, a partially depleted region consisting of SiC and a Si–O–C phase, is reported. The highest temperatures are achieved under arc-jet conditions, where typically very thick oxide layers with a very thin or no external glassy layer are reported for very short times. A depletion zone has also been observed under these conditions. Some works have suggested that convection currents can be significant during oxidation.[17–19] To obtain a quantitative model that interprets these data was the objective of this work.

In an initial study, we reported on a model for the oxidation of monolithic diborides of Zr and Hf in the temperature region of 1073–2673 K.[22–24] In the present work, we add the complexities arising from the presence of SiC and its oxidation products, silica and CO. We retain all the essential elements of the prior model, including volumetric effects from phase change of the oxide, and transitions in mechanistic regimes as temperature is increased.[24] As in the prior model, the refractory oxide in the scale is assumed to be impermeable to oxygen due to the known low electronic conductivity.[22] The effects of the presence of SiC are the formation of a borosilicate glass instead of a boria glass with all its consequences, the formation and transport of gaseous CO and SiO, and the evaporation of SiO and SiO_2 at the surface. The properties of silica and boria are known but modeling their variation with composition needs interpolation. The vapor pressures of B_2O_3 and SiO_2 are known as a function of temperature, and that of SiO is known as a function of temperature and oxygen partial pressure.

The model is able to interpret most of the experimental data reported on ultra-high temperature ceramics (UHTCs). Weight gain, oxide thickness, external glass thickness, and internal depletion layer thickness for both SiC–ZrB_2 and SiC–HfB_2 are found to be in reasonable agreement with experimental data, but with some exceptions mostly related to arc-jet test data. The equations that constitute the model are presented first; this is followed by a section where the predictions are compared with the available experimental data. The final section discusses the merits and limitations of the

N. Jacobson—contributing editor

Manuscript No. 29879. Received June 15, 2011; approved October 03, 2011.

This work was supported by USAF Contract # FA8650-10-D-5226 which included funding from US Air Force Office of Scientific Research (AFOSR), monitored by Dr. Ali Sayir.

[†]Author to whom correspondence should be addressed. e-mail: triplicane.parthasarathy@wpafb.af.mil

Report Documentation Page

Form Approved
OMB No. 0704-0188

1. REPORT DATE	2. REPORT TYPE	3. DATES COVERED
2012		**00-00-2012 to 00-00-2012**

4. TITLE AND SUBTITLE	5a. CONTRACT NUMBER
Modeling Oxidation Kinetics of SiC-Containing Refractory Diborides	5b. GRANT NUMBER
	5c. PROGRAM ELEMENT NUMBER
6. AUTHOR(S)	5d. PROJECT NUMBER
	5e. TASK NUMBER
	5f. WORK UNIT NUMBER
7. PERFORMING ORGANIZATION NAME(S) AND ADDRESS(ES) **Air Force Research Laboratory,Materials and Manufacturing Directorate,Wright-Patterson AFB,OH,45433-7817**	8. PERFORMING ORGANIZATION REPORT NUMBER
9. SPONSORING/MONITORING AGENCY NAME(S) AND ADDRESS(ES)	10. SPONSOR/MONITOR'S ACRONYM(S)
	11. SPONSOR/MONITOR'S REPORT NUMBER(S)

12. DISTRIBUTION/AVAILABILITY STATEMENT
Approved for public release; distribution unlimited

13. SUPPLEMENTARY NOTES

14. ABSTRACT

15. SUBJECT TERMS

16. SECURITY CLASSIFICATION OF:			17. LIMITATION OF ABSTRACT	18. NUMBER OF PAGES	19a. NAME OF RESPONSIBLE PERSON
a. REPORT	b. ABSTRACT	c. THIS PAGE			
unclassified	**unclassified**	**unclassified**	**Same as Report (SAR)**	**12**	

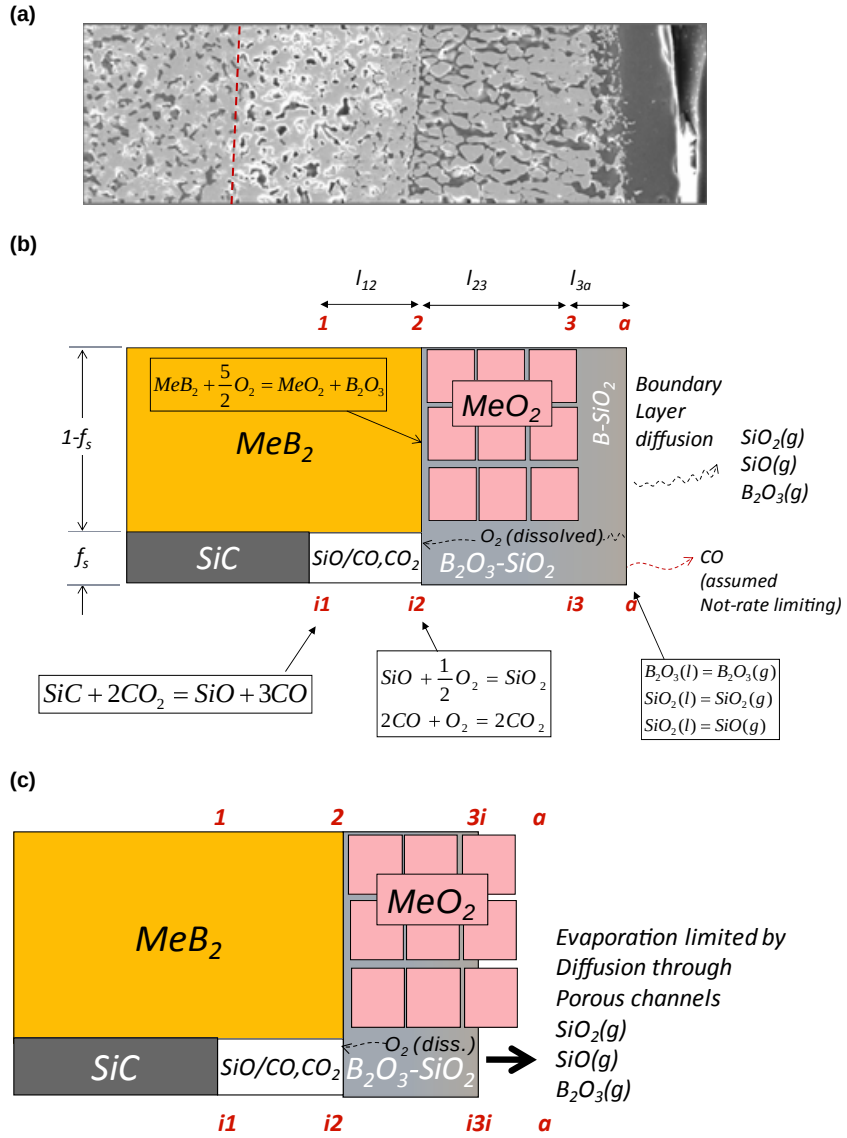

Fig. 1. (a) SEM image of the microstructure of oxidation scale formed on a ZrB_2–SiC sample (Courtesy: E Opila, Univ. Virginia) (b, c) Schematic sketches of the oxidation products and morphology assumed in the model. At lower temperatures (b) external glassy scale forms, whereas at higher temperatures or high ambient flow (c), the glassy scale recedes inward due to evaporative loss of SiO_2 and B_2O_3.

model, including possible reasons for discrepancies and suggestions for future work.

II. The Model

(1) Model Framework and Key Assumptions

The morphology of the oxidation scale assumed in the model was derived from published cross-sectional microstructures of oxidized UHTCs.[4,5,8,10,13,21,25] The key elements of the model are shown in Fig. 1. Figure 1(a) shows a sample microstructure of the scale formed on a ZrB_2–SiC material. The illustration, in Figs. 1(b) and (c), details the assumed morphology of the oxidation products, representing steady-state conditions. The substrate is a composite of SiC and MeB_2 (Me = Zr, Hf) with f_s being the volume fraction of SiC. The oxidation product, viz. the scale, consists of disconnected (in cross-section) MeO_2 grains with a continuous porous (void of solid) region that is filled with liquid borosilicate. Throughout the manuscript, pore refers to a region void of MeO_2 but filled with glass, except at very high temperatures when glass evaporates leaving pores behind [Fig. 1(c)]. The MeO_2 grains are taken to be impermeable to oxygen, as explained in our prior work.[22] Molecular oxygen from the ambient dissolves in borosilicate as molecular O_2, diffuses across the external glassy phase, and permeates through the porous channels of glass, eventually reaching the interface *i*2, where it reacts with the diboride. A portion of the oxygen flux, assumed to be proportional to areal (= volume) fraction of SiC, is transported within the depleted region (void of solid but filled with gases) to oxidize SiC through a medium of a gas mixture of CO and CO_2, similar to the model by Holcomb and St. Pierre for HfC oxidation.[26] The gaseous reaction product, CO, of the SiC oxidation is assumed to either diffuse or bubble through the glassy scale (as observed in ref. 17–19) and is assumed not to be rate limiting, consistent with prior assumptions for oxidation of SiC.[27] Figure 1(b) depicts the expected scenario at higher temperatures (likely above 2000 K) where evaporation of B_2O_3 and SiO_2 from the external surface is sufficiently high that an external glassy layer cannot be supported and the glassy layer recedes inwards. In all regimes, the diffusivity of gases in a multicomponent gas mixture and the effect of Knudsen diffusion [when an unfilled pore was present as in Fig. 1(b)] were modeled as detailed in prior work.[22]

The volume fraction of SiC in the substrate is f_s, and the volume fraction of porosity (filled with glass) within the MeO_2 region is f_p. As in prior work, the pore fraction, f_p, (filled with glass) is taken to change as the temperature crosses the monoclinic–tetragonal phase transformation temperature, T_{trans}. The parameters f_s and f_p are related to the volume fraction,

f_{MeO_2}, of MeO_2 in the glass + MeO_2 region (2–3), and fraction of glass, f_g, (borosilicate) in the scale as follows.

$$\begin{aligned} f_p &= f_1 \text{for } T < T_{trans} \text{ and } f_2 \text{ for } T > T_{trans} \\ f_g &= f_s + f_p(1-f_s) \\ f_{MeO_2} &= (1-f_p)(1-f_s) = 1-f_g \end{aligned} \quad (1)$$

As shown in Fig. 1, $(1 - f_s)$ is the volume fraction of MeB_2 and $(1 - f_p)$ is the volume fraction of MeO_2 within the MeO_2 + glass layer (region 2–3). Thus, when no SiC is present (monolithic MeB_2), $f_g = f_p$. In the presence of SiC, the glass volume fraction is increased by f_s.

The B_2O_3 activity, $a_{B_2O_3-i2}$, of the borosilicate scale at the MeB_2–MeO_2 interface, denoted by the subscript $_{i2}$, is derived in terms of the recession rate of the MeB_2 phase, $\frac{dR_{MeB_2}}{dt}$, and that of the SiC phase, $\frac{dR_{SiC}}{dt}$. Accounting for their phase fractions and their molar volumes, V_{MeB_2}, V_{SiC} of MeB_2 and SiC, and assuming an ideal mixture, we obtain:

$$\begin{aligned} a_{B_2O_3-i2} &= \frac{\frac{(1-f_s)}{V_{MeB_2}}\left(\frac{dR_{MeB_2}}{dt}\right)}{\frac{(1-f_s)}{V_{MeB_2}}\left(\frac{dR_{MeB_2}}{dt}\right)+\frac{f_s}{V_{SiC}}\left(\frac{dR_{SiC}}{dt}\right)}; \\ a_{SiO_2-i2} &= 1 - a_{B_2O_3-i2} \end{aligned} \quad (2)$$

Here, the activity is taken to be directly proportional to molar ratio, assuming an ideal behavior. This assumption is fairly consistent with the work of Boike *et al.*, who reported only a slight positive deviation from ideal behavior and the experimental work of Kawamoto *et al.*, who found no phase separation in this B_2O_3–SiO_2 system.[28,29]

The equilibrium constant for the oxidation of diboride is related to the boria activity and oxygen partial pressure at interface *i*2 and is given by:

$$\begin{aligned} &\text{At } i2: MeB_2 + \frac{5}{2}O_2 = MeO_2 + B_2O_3; \\ &K_{Me} = \frac{a_{MeO_2}\, a_{B_2O_3-i2}}{a_{MeB_2}(P_{O_2-i2})^{5/2}}; \end{aligned} \quad (3)$$

where K refers to equilibrium constant, a the activity, and P the partial pressure, whereas subscripts refer to species and the interface *i*2 shown in Fig. 1.

(2) Internal Depletion Region (1–2)

Due to the low oxygen partial pressure at interface *i*2, the only way SiC can oxidize at interface *i*1 behind *i*2, is if oxygen was transported across the void by CO/CO_2 counter diffusion. Likewise, a gaseous SiO(*g*) from oxidation of SiC, transports Si to sustain the glassy oxidation product at *i*2. The oxygen dissolved in the glass at the interface *i*2 reacts with CO(*g*) to form CO_2(*g*) which diffuses across region (1–2) to oxidize SiC at interface *i*1. The SiO(*g*) formed at interface *i*1 diffuses back to interface *i*2 where it is oxidized by the dissolved oxygen in the glass. This model yields the following reactions with associated equilibrium constants.

$$\begin{aligned} &\text{At } i2: SiO(g) + \frac{1}{2}O_2(\text{dissolved}) = SiO_2; \\ &\quad 2CO(g) + O_2(\text{dissolved}) = 2CO_2(g) \\ &\text{Combining}: SiO(g) + 2CO(g) + \frac{3}{2}O_2(\text{dissolved}) \\ &\quad = SiO_2 + 2CO_2(g) \\ &\text{At } i1: SiC + 2CO_2(g) = SiO(g) + 3CO(g) \end{aligned}$$

$$\begin{aligned} K_{SiO} &= \frac{a_{SiO_2-i2}}{P_{SiO-i2}(P_{O_2-i2})^{1/2}}; \\ K_{SiC} &= \frac{P_{SiO-i1}(P_{CO-i1})^3}{P_{SiC}(P_{CO_2-i1})^2}; \\ K_{CO_2} &= \frac{(P_{CO_2-i2})^2}{(P_{CO-i2})^2 P_{O_2-i2}} \end{aligned} \quad (4)$$

At steady state, the fluxes of the gaseous species within the depleted zone (between *i*1 and *i*2) must be decided and be consistent with the equilibrium constants of Eqs. (4), and the oxidation rate is limited by incoming oxygen flux at *i*2, J_{O_2-32} times the area fraction, f_s, of SiC at the interface *i*2. Thus, for the depleted zone, we obtain:

$$\begin{aligned} &|J_{CO-12}| = \frac{3}{2}|J_{CO_2-21}|; \quad |J_{SiO-12}| = \frac{1}{2}|J_{CO_2-21}|; \\ &|J_{SiO-12}| = \frac{2}{3}f_s|J_{O_2-32}| \\ &|J_{CO_2-21}| = f_s\frac{D_{CO_2-12}}{RT}10^5\frac{P_{CO_2-i2}-P_{CO_2-i1}}{l_{12}}; \\ &|J_{CO-12}| = f_s\frac{D_{CO-12}}{RT}10^5\frac{P_{CO-i1}-P_{CO-i2}}{l_{12}} \end{aligned} \quad (5)$$

In these expressions, J is the flux in moles per unit area per unit time, D the diffusivity, R the universal gas constant, T the absolute temperature, and l_{12} is the length of the depleted zone. The factor 10^5 refers to conversion from atm to Pascal. The first subscript used in all the quantities refers to the species. The second subscript used with partial pressures refers to the interface, while that used with diffusivity and flux refers to the regions between interfaces.

There are seven unknowns that describe region 1–2, of which the oxygen partial pressure at *i*2 is given by Eq. (3). The remaining six unknowns, the partial pressures of the three species (CO, CO_2, and SiO) at the two interfaces *i*1 and *i*2, are obtained by solving the Eqs. (4) and (5). Thus, we obtain the following expressions for these six unknowns. They are presented in algorithmic sequence, wherein each variable can be calculated from a knowledge of all preceding variables.

$$\begin{aligned} &P_{O_2-i2} = \left(\frac{a_{MeO_2}\, a_{B_2O_3-i2}}{a_{MeB_2}K_{Me}}\right)^{2/5}; \quad P_{SiO-i2} = \frac{a_{SiO_2-i2}}{K_{SiO}\sqrt{P_{O_2-i2}}}; \\ &P_{SiO-i1} = \frac{2RT|J_{O_2-32}|l_{12}}{3\times 10^5 D_{SiO-12}} + P_{SiO-i2} \end{aligned}$$

$$\begin{aligned} &P_{CO-i1}(D_{CO-12}D_{CO_2-12}\sqrt{K_{CO_2}P_{O_2-i2}}) \\ &-(P_{CO-i1})^{3/2}D_{CO-12}D_{CO_2-12}\sqrt{\frac{K_{CO_2}P_{SiO-i1}}{K_{SiC}}} \\ &-2D_{CO-12}D_{SiO-12}P_{SiO-i1} \\ &-3D_{CO_2-12}D_{SiO-12}\sqrt{K_{CO_2}P_{O_2-i2}}P_{SiO-i1} \\ &+2D_{CO-12}D_{SiO-12}P_{SiO-i2} \\ &+3D_{CO_2-12}D_{SiO-12}\sqrt{K_{CO_2}P_{O_2-i2}}P_{SiO-i2}=0 \\ &P_{CO_2-i1}=\frac{(P_{CO-i1})^{3/2}\sqrt{P_{SiO-i1}}}{\sqrt{K_{SiC}}} \\ &P_{CO-i2}=\frac{D_{CO-12}P_{CO-i1}-3D_{SiO-12}P_{SiO-i1}+3D_{SiO-12}P_{SiO-i2}}{D_{CO-12}} \\ &P_{CO_2-i2}=P_{CO-i2}\sqrt{K_{CO_2}P_{O_2-i2}} \end{aligned} \quad (6)$$

One of them, $P_{CO\text{-}i1}$, requires numerical solution of the implicit equation. The only unknowns in the above equation set are the oxygen flux, $|J_{O_2-32}|$, in the region 2–3 (Fig. 1), and the length of the depleted zone, l_{12}. The flux $|J_{O_2-32}|$ is obtained from solving the equations that apply to region 2–3, discussed below.

(3) MeO_2 + B_2O_3–SiO_2 Glass Region (2–3)

The equations that govern the oxygen flux in region 2–3, between interfaces $i2$ and $i3$, are given below.

$$
\begin{aligned}
&|J_{O_2-32}| = \Pi_{O_2-B_2O_3-SiO_2}\frac{P_{O_2-i3}-P_{O_2-i2}}{l_{23}}f_g\\
&|J_{O_2-a3}| = \Pi_{O_2-B_2O_3-SiO_2(3a)}\frac{P_{O_2-a}-P_{O_2-i3}}{l_{3a}}\\
&\text{Since,} |J_{O_2-a3}| = |J_{O_2-32}|\\
&P_{O_2-i3} = \frac{l_{23}\Pi_{O_2-B_2O_3-SiO_2(3a)}P_{O_2-a}+f_g l_{3a}\Pi_{O_2-B_2O_3-SiO_2}P_{O_2-i2}}{l_{23}\Pi_{O_2-B_2O_3-SiO_2(3a)}+f_g l_{3a}\Pi_{O_2-B_2O_3-SiO_2}}
\end{aligned}
\tag{7}
$$

Here, Π refers to the permeability (rate of transport in moles per unit area per unit time per unit partial pressure gradient). The permeability in region 3-*a* is different from that in region 2–3, as region 3-*a* is likely to be a boria-deficient region resulting from faster evaporation of boria than silica.

The unknowns that remain are the three lengths, l_{12}, l_{23}, and l_{3a} of the three regions. These are allowed to evolve with time from an initially small value within a numerical simulation model. The evolution equations for l_{12} and derived from flux and molar volumes are given below. The rate of change of l_{23} is given by the number of moles of MeO_2 formed per unit area per unit time multiplied by the molar volume of MeO_2. The rate of formation of MeO_2 is given by the total flux of oxygen in through region 3–2, less than that used for oxidizing SiO(*g*) to SiO_2 and CO(*g*) to CO_2, which is 3/2 times the SiO(*g*) flux in region 1–2 as given in Eq. 4. The recession rate of MeB_2 and SiC are simply related to the rate of change of l_{23} through molar volumes and volume fractions. Finally, the depleted zone length change is given by the difference in recession between MeB_2 and SiC. Thus, we obtain the following equations.

$$
\begin{aligned}
&\frac{dl_{23}}{dt} = V_{MeO_2}\left(|J_{O_2-32}| - \frac{3}{2}|J_{SiO-12}|\right)\frac{2}{5}\frac{1}{f_{MeO_2}}\\
&\frac{dR_{MeB_2}}{dt} = \frac{dl_{23}}{dt}\frac{V_{MeB_2}f_{MeO_2}}{V_{MeO_2}(1-f_s)}\\
&\frac{dR_{SiC}}{dt} = |J_{SiO-12}|\frac{V_{SiC}}{f_s}\\
&l_{12} = R_{SiC} - R_{MeB_2}
\end{aligned}
\tag{8}
$$

In the above set of equations, t is time, R is recession, V is molar volume, and J is flux (moles per unit area per unit time).

(4) External B_2O_3–SiO_2 Glass Region (3-a)

The evolution with time for the thickness, l_{3a}, of the external glassy layer 3-*a*, is given by the rate of production of boria and silica less the rate of loss by evaporation at the surface and the amount occupied by glass in region 2–3. From the literature, B_2O_3(*g*), SiO(*g*), and SiO_2(*g*) are known to be the dominant gaseous species in the B_2O_3–SiO_2 system in the temperature and oxygen partial pressures of interest (see for example, ref. 7).

$$
\begin{aligned}
&\frac{dl_{3a}}{dt} = \left(\frac{dl_{23}}{dt}\frac{f_{MeO_2}}{V_{MeO_2}} - \left|J_{B_2O_3-vap}\right|\right)V_{B_2O_3} + (|J_{SiO-12}|\\
&- \left|J_{SiO_2-vap}\right| - \left|J_{SiO-vap}\right|)V_{SiO_2} - \frac{dl_{23}}{dt}f_g\\
&\left|J_{species-vap}\right| = \frac{D_{species}}{RT}10^5\frac{P_{species-vap}}{\delta_{bdry}};\delta_{bdry}\\
&= \frac{3}{2}\sqrt{\frac{l_{specimen}}{v_{fluid}}}\left[\frac{\eta_{flfluid}}{\rho_{fluid}}\right]^{1/6}(D_{species})^{1/3}
\end{aligned}
\tag{9}
$$

In the above equation set, the subscript 'vap' refers to evaporation, $l_{specimen}$ is the length of the specimen, η, ρ, and v refer to viscosity, density, and velocity of the ambient fluid. The last equation gives the boundary layer (thickness δ)-dependent evaporation of species.[30]

The viscosity of the glassy layer could limit the maximum thickness, $l_{3a\text{-max}}$, of the external layer that can be supported under gravitational forces. As in the previous work,[24,31] from the theory of falling liquid films,[31] under laminar flow, this limiting thickness is given by:

$$
\begin{aligned}
&l_{3a-max} = \left[\frac{3(M_{B_2O_3-SiO_2}\Gamma_{B_2O_3-SiO_2}l_{spec})\eta_{B_2O_3-SiO_2}}{g\rho^2_{B_2O_3-SiO_2}\sin(\phi)}\right]^{1/3}\\
&\Gamma_{B_2O_3-SiO_2} = \frac{dl_{3a}}{dt}\frac{1}{V_{B_2O_3-SiO_2}}
\end{aligned}
\tag{10}
$$

where subscript B_2O_3–SiO_2 refers to the borosilicate present at the surface region (3-a), M refers to molecular weight, g the acceleration due to gravity, φ the orientation of the sample with respect to gravity, and $\Gamma_{B_2O_3-SiO_2}$ refers to the rate at which the borosilicate is added to the surface in moles per unit area per unit time.

Finally, the net weight gained, weight of oxygen consumed, and weight evaporated can be given as:

$$
\begin{aligned}
W_g &= l_{23}(f_{MeO_2}\rho_{MeO_2} + f_g\rho_g) + l_{3a}\rho_g\\
&\quad - R_{SiC}f_s\rho_{SiC} - R_{MeB_2}(1-f_s)\rho_{MeB_2}\\
W_{O_2} &= \frac{5}{2}R_{MeB_2}\frac{(1-f_s)}{V_{MeB_2}}M_{O_2} + \frac{3}{2}R_{SiC}\frac{f_s}{V_{SiC}}M_{O_2}\\
W_{evap} &= \sum_{(SiO_2,SiO,B_2O_3)}M_{species}\int_0^t J_{species}dt + \frac{R_{SiC}f_s}{V_{SiC}}M_{CO}
\end{aligned}
\tag{11}
$$

The variation in time of the oxide scale thicknesses and the various weight gain/loss can be computed numerically using Eqs. (1)–(11) using an evolutionary algorithm which is started with a choice of, initially, arbitrarily small value for l_{12}, l_{23}, and l_{3a}.

(5) High-Temperature Regime

At high temperatures (likely above 2000 K) and/or at high flow rates of ambient fluid (>1 m/s), where the evaporation rates of SiO_2(*g*) and/or SiO(*g*) are sufficiently high, the external glassy layer will be lost and the glassy liquid region will recede into the region 2–3, as shown in Fig. 1(b). Using 3*i* to identify the location of the receding glassy layer, the following equations describe the oxygen flux balance which fixes the partial pressure of oxygen, P_{O_2-i3i}, at the interface $i3i$ at the location 3*i*,

$$J_{O_2-3i2} = \Pi_{O_2-B_2O_3-SiO_2} \frac{P_{O_2-i3i} - P_{O_2-i2}}{q l_{23}} f_g$$
$$J_{O_2-a3i} = \frac{D_{O2-3ia}}{RT} 10^5 \frac{P_{O_2-a} - P_{O_2-i3i}}{(1-q) l_{23}} f_g \text{ Since } J_{O_2-a3i} = J_{O_2-3i2} \quad (12)$$
$$P_{O_2-i3i} = \frac{qRT\Pi_{O_2-B_2O_3-SiO_2} P_{O_2-i2} - 10^5 q D_{O_2-3ia} P_{O_2-a} - RT\Pi_{O_2-B_2O_3-SiO_2} P_{O_2-i2}}{qRT\Pi_{O_2-B_2O_3-SiO_2} - 10^5 q D_{O_2-3ia} - RT\Pi_{O_2-B_2O_3-SiO_2}}$$

The diffusive fluxes of gaseous species (SiO_2, B_2O_3, and SiO) determine the rate of recession of the interface *i3i*. Taking the ratio of the depth of the glassy region to the length l_{23} of region 2–3 as q, the evolution equation for q is given as:

$$J_{species-vap} = \frac{D_{species-3ia}}{RT} 10^5 \frac{P_{species-vap}}{(1-q) l_{23}}$$
$$\frac{dq}{dt} = \frac{1}{l_{23}} \left[\frac{1}{f_g} \{ J_{SiO-12} V_{SiO_2} + (J_{O_2-3i2} - \frac{3}{2} J_{SiO-12}) \frac{2}{5} V_{B_2O_3} - J_{SiO_2-vap} V_{SiO_2} - J_{B_2O_3-vap} V_{B_2O_3} \} - q \frac{dl_{23}}{dt} \right] \quad (13)$$

The right-hand side of the evolution equation is the rate of production of B_2O_3 and SiO_2 less the evaporative flux; the last term accounts for the increase in l_{23} during the time increment. The weight gain of the sample is given as:

$$W_g = q l_{23} (f_{MeO_2} \rho_{MeO_2} + f_g \rho_g) - R_s f_s \rho_{SiC} - R_{MeB_2} (1 - f_s) \rho_{MeB_2} \quad (14)$$

Again, the variation in time of the oxide scale thickness and the weight gain/loss can be computed using an evolutionary algorithm.

III. Model Predictions and Validation

A numerical code written in Fortran was used for all the model predictions shown in this work. The input variables are the temperature–time history, environment parameters (total pressure, fraction of oxygen), specimen orientation, length, fluid velocity, volume fraction of SiC, size of SiC particles. All the thermodynamic and kinetic parameters taken from the literature reside within the code; these include oxygen permeation and viscosity of silica and boria, equilibrium constants for all the reactions, and vapor pressures of the species. An infinitesimal layer of oxide and a glassy layer were assumed present at an infinitesimal start time and the time evolution of all the parameters were calculated as dictated by the equations. An arbitrary time–temperature profile could be thus simulated and the resulting thicknesses of oxide, glassy layer, and depleted layer could be computed. From these, the recession, the weight gain, weight of oxygen consumed, and weight of evaporated species could be computed.

(1) Parameters

A list of variables used in the model is shown in Table I with a brief description. The model uses data from the literature for all thermodynamic quantities, viz. equilibrium constants and vapor pressures of species, which are available in the compendium by Barin.[32]

(A) Gas Diffusivity: The diffusivities of gases in a multigas solution were calculated using parameters given by Svehla,[33] and the methods outlined in Ref. 22 The gas diffusivity applied to the depleted region as well as the boundary layer diffusion region at the surface for evaporation. The Knudsen effect on diffusivity was included as determined by the pore radius, assumed to be 0.5 μm in all predictions shown herein; this choice was based on reported microstructures in the literature. The Knudsen effect only comes in when the pores dry out under conditions where the evaporation is sufficiently fast [Fig. 1(c)]. The Knudsen effect is also calculated for the depleted zone as determined by SiC size.

(B) Boria Activity: The calculation of equilibrium partial pressure of oxygen at the ZrB_2–ZrO_2 interface (*i2*) and the partial pressures of volatile species at the outer surface require the activity of boria in the borosilicate glass. The activity isotherm in the boria–silica system was measured at 1475 K and is found to be nearly ideal, although there is a slight deviation from ideality.[28] The B_2O_3–SiO_2 system is also known for the lack of any phase separation.[34] Based on these, a unit activity coefficient was assumed in this work.

(C) Glass Viscosity: The temperature-dependent viscosity of boria was obtained from the works of Eppler and Li *et al.*[35,36] The data on viscosity of silica were reviewed by Doremus,[37] and as per his conclusion, the data of Urbain *et al.*[38] were used for the temperature range 1400°C–2500°C and that of Hetherington *et al.*[39] for the temperature range 1400°C–1000°C. For compositional dependence of viscosity on boria content, a log-mean interpolation scheme was used consistent with semiempirical models of glass viscosities.[40,41]

(D) Oxygen Permeability: The permeabilities of oxygen in liquid boria and silica were obtained by fitting to data from several sources. The boria data were obtained from Tokuda *et al.*,[42] Luthra,[43] and Schlichting.[44] The oxygen permeability in silica was obtained from the works of Lamkin *et al.*[45] and Courtright.[46] For the compositional dependence, a log-mean approximation was used for interpolation consistent with what might be expected from Stokes–Einstein relation as suggested by Karlsdottir and Halloran.[17]

The boria concentration at the surface layer must be lower than that in the interior oxide + glass region due to evaporative losses of boria being higher than silica. The surface layer concentration depends on the evaporative rates, diffusion of B in B-SiO_2, and the degree of convective mixing. This calculation is beyond the scope of this work. Further, the authors have found no experimental data on this. Hence, the surface boria concentration was assumed to be a constant fraction of the interior (interior B_2O_3 concentration is ~0.72 for 20% SiC); this was the only loose parameter in the model and values of 0.8 and 0.9 (B_2O_3 concentration of ~0.58 and ~0.65) for HfB_2 and ZrB_2, respectively, gave the best correspondence. The effective pore fractions, f_p, for zirconia and hafnia were taken to be the same as was in ref. 24 for monolithic diboride oxidation (0.03 and 0.04 for HfO_2 and ZrO_2, respectively). The aliovalent dopant concentration, C_{dopant}, in MeO_2 was taken to be less than 100 ppm, which permits the neglect of oxygen permeation through the MeO_2 phase (an excellent assumption) (see ref. 22–24). The ambient fluid velocity was obtained from the literature when reported; it varied from 0.0001 to 150 m/s, with the smaller values corresponding to static air, and the higher values close to arc-jet conditions (behind the shock wave). The effect of fluid flow on evaporation rates was included in the model using a

Table I. A List of Symbols Used in This Work, with a Brief Description and Units

Symbol	Units	Description
f_p		Effective volume fraction of pores in MeO_2 that is permeable to gas
f_s		Volume fraction of SiC
f_{MeO2}		Volume fraction of MeO_2 in the MeO_2–glass region (2–3)
f_g		Volume fraction of glass region in the MeO_2–glass region (2–3)
$a_{species\text{-}i2}$		Activity of species at interface *i*2
R_{MeB2}	m	Recession of MeB_2
R_{SiC}	m	Recession of SiC
$V_{species}$	m^3	Molar volumes of species
$P_{species}$	atm	Partial pressure of species
$J_{species\text{-}12}$	mol/m^2-s	Flux of species from interface 1–2
$D_{species\text{-}12}$	m^2/s	Diffusivity of species in region 1–2
R	J/mol-K	Universal gas constant
$\Pi_{O_2-B_2O_3-SiO_2}$	mol/m-s-atm	Permeability coefficient of oxygen in liquid borosilicate
I_{12}	m	Depth of internal depletion ($=R_s - R_{me}$)
l_{23}	m	Thickness of zirconia region in the scale
I_{3a}	m	Thickness of external glassy layer of B_2O_3–$SiO_2(l)$
q	m	Thickness of zirconia scale over which B_2O_3–$SiO_2(l)$ is present
T	K	Temperature
t	s	Time
M_i	kg/mol	Molecular weight of species *i*
ρ_i	kg/m^3	Density of species *i*
η_i	Pa-s	Viscosity of species *i*
$\Gamma_{B_2O_3-SiO_2}$	mol/m^2-s	Rate of addition of boria to the external boria scale
$J_{species\text{-}vap}$	mol/m^2-s	Rate of evaporation of species *i* at the external surface
δ_{bdry}	m	Boundary layer thickness for surface evaporation
$I_{specimen}$	m	Length of specimen
V_{fluid}	m/s	Velocity of ambient fluid
W_g	kg/m^2	Net change in weight per unit area
W_{O_2}	kg/m^2	Weight of O_2 consumed per unit area
W_{evap}	kg/m^2	Weight of evaporated species per unit area

boundary layer calculation (as detailed in ref. 22–24), but the possible thinning of the external glassy layer from shear forces was not included in the model.

(2) Comparison of Model Predictions with Experimental Data

(A) SiC: There are a lot of oxidation data for SiC in the literature, and comparing the model to these data is important as a first check. As the oxygen permeability in silica was used in the model, the comparison of model to data must be taken as validation of the assumption that the kinetics of oxidation is limited by oxygen permeability in the glassy phase, at least for SiC. Figure 2 shows a plot that compares the available data for single and polycrystalline SiC in various forms reported by different investigations[47–53] in pure oxygen; there is a large scatter in the data. Figure 2 includes data collected on high purity SiC by Ramberg *et al.*,[47] and Ogbuji and Opila[53] as well as data obtained by a Costello and Tressler[49] on SiC made by different processing methods. The model is seen to fit fairly well with the polycrystal data, and the fast oxidizing (Si face) data for the single crystal.

(B) SiC–ZrB_2: A comprehensive work on the effect of SiC content on the oxidation kinetics of UHTCs was performed by Talmy.[54] The study was conducted using a thermogravimetric apparatus in flowing air. The weight gain of samples exposed for 2 h in air is reported. In a more recent work, Wang *et al.*[15] have conducted a similar study using SiC volume fractions of 0, 5, 10, 15, and 20 vol% at temperatures up to1600°C for 1h in an air furnace. Figure 3 compares the data with the model prediction for weight gain as a function of SiC volume percent. Figure 3(a) shows data from Talmy[54] and Fig. 3(b) shows data from Wang *et al.*[15] The model predictions for the sample weight gain and the total weight of oxygen consumed are shown as solid and dashed

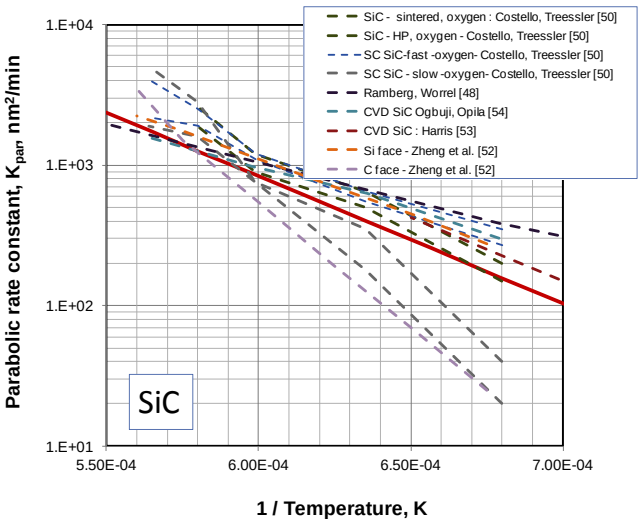

Fig. 2. The oxidation kinetics, expressed as parabolic rate constant, in oxygen of single crystal and polycrystal SiC in various forms reported by various investigators are shown compared with the model. The model prediction is shown as a solid line, whereas the experimental data are shown as dotted lines.

lines. The sample weight gain is the weight of the sample and oxidation products less the weight of external glassy phase predicted to be lost by evaporation or viscous flow. The weight of oxygen consumed will be the total weight change if all of the oxidation products were retained on the sample. Figure 3(c) includes time dependence data at 1200°C from Wang *et al.* The model agrees with the trends very well.

The temperature dependence of weight gain and scale thickness data on a fixed composition of 20 vol%SiC–ZrB_2

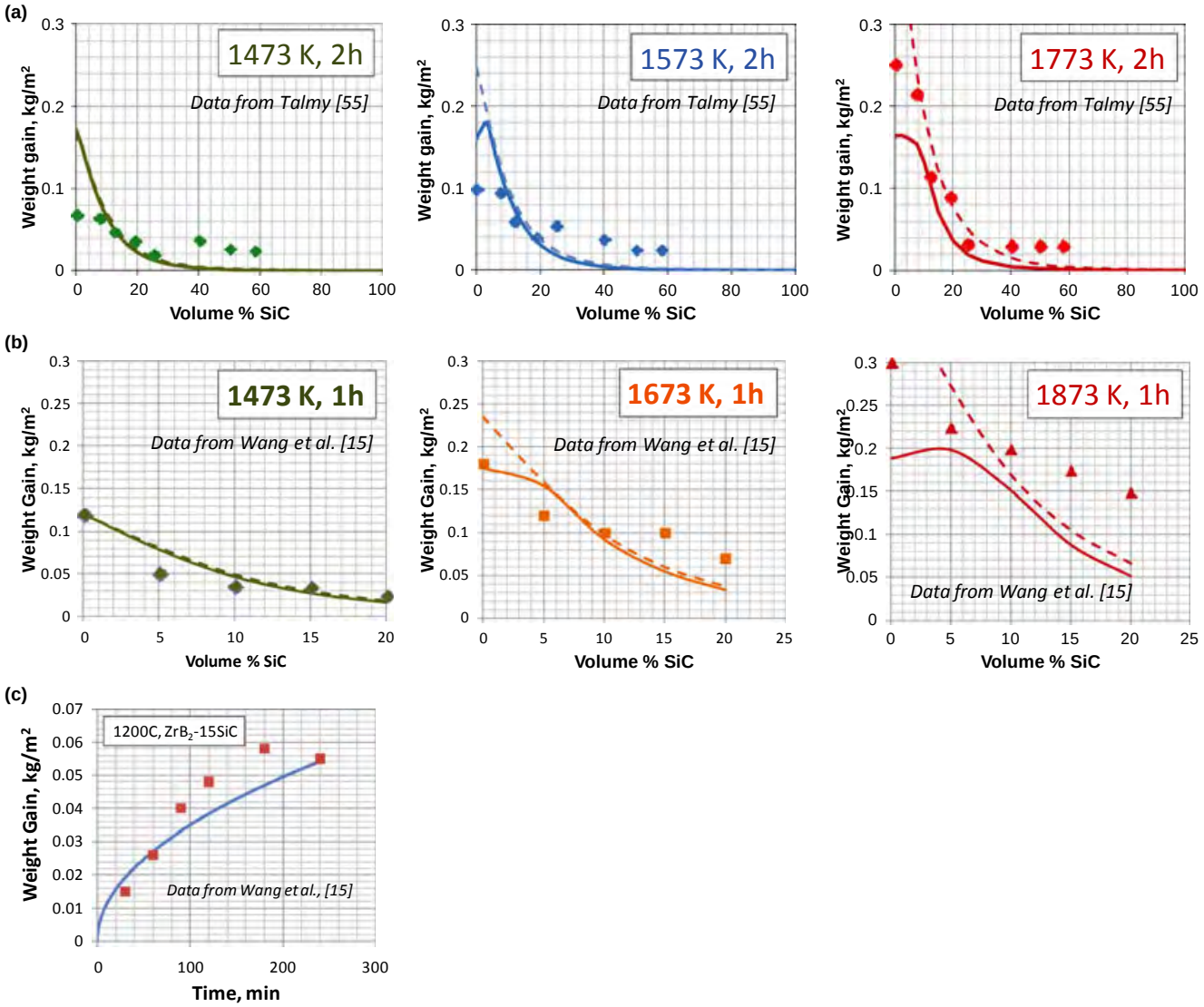

Fig. 3. (a) The effect of volume percent SiC on the oxidation weight gain in 2 h of UHTC ($SiC–ZrB_2$) samples, as measured by Talmy[54] shown compared with the prediction of the model for three different temperatures. The solid lines are the predictions that include the flow of external glassy layer under gravity and evaporation of boria or silica. The dotted lines show the predicted weight of oxygen consumed, which is the maximum weight gain that the samples could have suffered from oxidation in the absence of flow/evaporation of the glassy layer. In (b), the model is shown compared with data from a different investigation, by Wang *et al.*,[15] which used a 1-h hold at temperature. In (c), the weight gain as a function of time for a ZrB_2–15 vol%SiC sample at 1200°C reported by Wang *et al.*[15] is shown compared with the model.

in static laboratory air have been reported by Carney *et al.*[10] This study took special care to document the effect of glass flow in two ways. They measured the weight changes of both the sample and the crucible onto which some of the glass had spread. They also measured the variation in scale thickness with sample surface orientation, and found significant scatter. Further, they reported on samples prepared by SPS and hot press. For comparison with the model, the average values of all the samples for a given condition were used. The experimental data points attributed to Opila and Halbig in Fig. 4(a) were calculated from the parabolic constants for weight gain reported in their work.[13] In Fig. 4(a), the total weight gain (sample + crucible) is plotted along with the model predictions, showing good correspondence. The plot also shows that evaporation is significant above 1873 K. Figure 4(b) shows the average values for total scale (oxide + glass) thicknesses and oxide thicknesses. Figure 4(b) includes scale thicknesses data measured from images reported by Zhang *et al.*[14] The data of Carney were obtained in an alumina furnace whereas the data of Zhang *et al.* were obtained using a zirconia furnace. A clear internal depletion layer was not observed/reported in the experiments. In contrast, Fahrenholtz [7] reported a depletion layer of 10 μm after 30 min at 1773 K in a ZrB_2–30% SiC sample; the model predicts only 0.6 μm for these conditions. For the 20% $SiC–ZrB_2$ case, the model predicts a depletion zone ranging from 1.8 μm at 1673 K to 3 μm at 1873 K which is closer to observations by Carney *et al.* Figure 5 shows a comparison of the model with data for the time dependence of weight gain and scale thickness from two sources of data.[5,10] Data for hot-pressed samples and SPS-processed samples and the sources of the data are distinguished with different symbol shapes. Once again, there is a reasonable correspondence between the data and the model.

(C) SiC–HfB_2: Oxidation data on SPS-processed high-density 20 vol%$SiC–HfB_2$ samples have been collected in static air from 1673 to 2273 K by Carney.[11] In addition, the statistical variations from batch to batch and processing route (hot-pressed versus SPS) have been studied for the same composition at 1773 and 1873 K by Sevener.[20] Figure 6(a) compares the data for weight gain with the model predictions. The data for weight gain include separate measurements for the sample (open symbols) and crucible + sample (filled symbols). The model predictions include

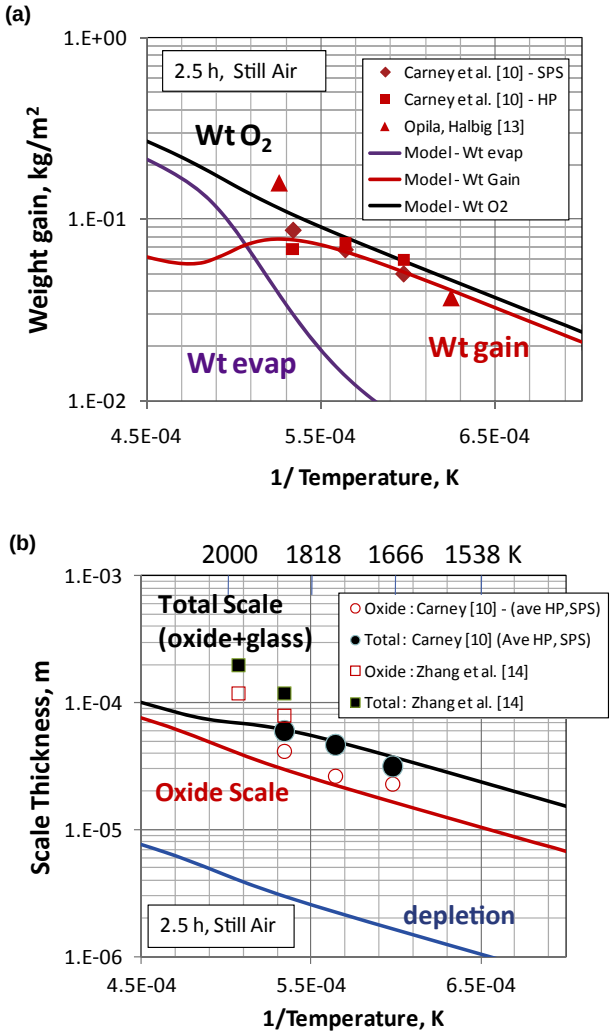

Fig. 4. (a) Oxidation weight gain in ZrB_2–20 vol%SiC samples, measured in static air after 2.5 h of exposure, by Carney *et al.*[10] shown compared to the model predictions. The data from Opila and Halbig[13] are also shown. The solid lines are model predictions for weight gain, weight of oxygen consumed, and weight evaporated. (b) Average of reported values for the oxide scale thickness (open symbols) and total (oxide + glass) scale thickness (filled symbol) for the same exposures; values measured on different sides of the samples were averaged for this plot. Values from the work of Zhang *et al.*[14] which used a zirconia furnace, are also included. The solid lines are predictions for total scale, oxide scale, and depletion thicknesses. No depletion thickness was reported, but partial depletion was noticed under FIB/TEM investigation.[10]

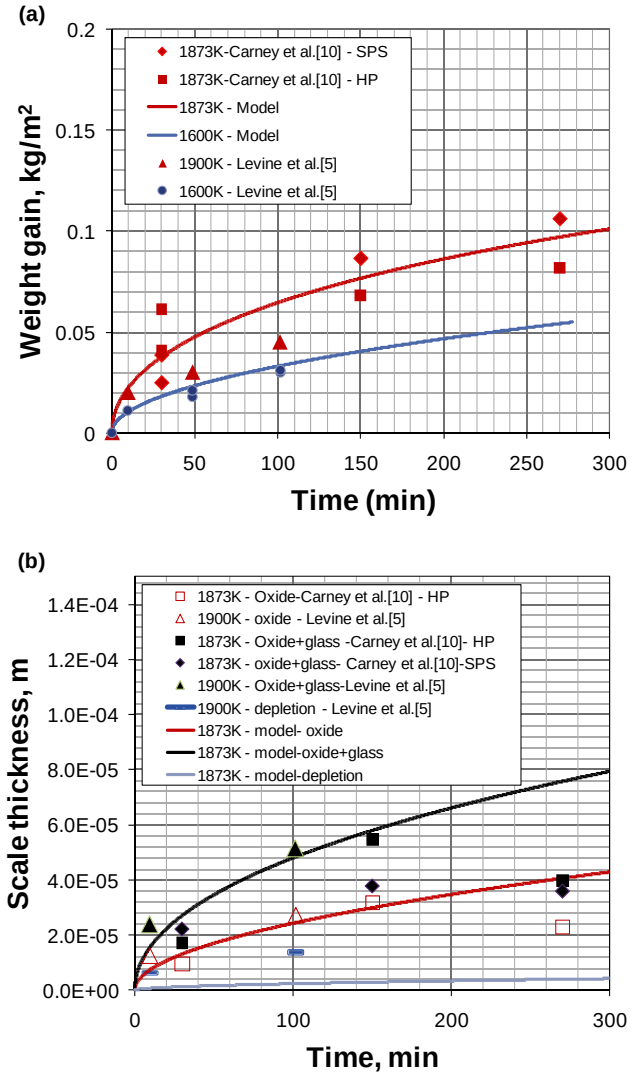

Fig. 5. (a) Model compared with oxidation weight gain measured as a function of time during oxidation of ZrB_2–20 vol%SiC samples in static air at 1873 K, by Carney *et al.*[10] and at 1900 and 1600 K by Levine *et al.*[5] The solid lines are model predictions for the two temperatures. (b) Model compared with reported oxide thickness (open), total (oxide + glass) thickness (filled), and internal depletion thickness (dash) as marked. In both (a) and (b), the squares represent Carney's hot-pressed samples, the diamonds Carney's SPS samples, and triangles data from Levine *et al.*

total weight of oxygen consumed, sample weight gain, and weight evaporated. Evaporation is predicted to dominate at around 2000 K, and the model is consistent with the drop in sample weight gain at this temperature. In general, the model captures the trends well except at the highest temperature. In Fig. 6(b), the scale thicknesses measured are compared with the model. The microstructures of the oxidation product were complex at the highest temperatures, and there was ambiguity in the definition of the depleted zone. Thus, the sum of oxide scale and depletion zone (open symbols) was used for this comparison. The total scale thicknesses (filled symbols) are also plotted. The correspondence between the model and data is seen to be reasonable, except for the data at the highest temperature reported, viz. 2173 K, which deviates significantly from the model. However, these data also deviate significantly from the extrapolation of the data at lower temperatures. On further examination of the sample, significant contamination of alkali elements (mainly Ca) possibly from the furnace or crucible (Ca-stabilized zirconia) was detected. Enhanced oxidation of SiC due to the presence of impurities is well known (for example, see Ramberg *et al.*[47])

Figure 7 compares the model predictions for weight gain as a function of time for 20 vol%SiC–HfB_2 in furnace air at 1773 and 1873 K, with data reported by Sevener.[20] The data include SPS-processed material and hot-pressed material with different initial SiC particle sizes obtained from different processing routes. The data reported for the combined weight gain of sample and crucible were used. The correspondence is once again found to be good, although there is considerable scatter in the data. The model prediction plotted in Fig. 7 includes the total weight of oxygen consumed showing that evaporative loss becomes significant at 1873 K.

(D) Arc-Jet Tests on SiC–MeB_2: The expense of conducting arc-jet tests has limited the number of investigations and the extent of data available on oxidation kinetics during these tests. However, data are available for a few SiC–MeB_2 compositions. Montverde and Savino have tested a hemispherical sample of ZrB_2–15 vol%SiC under arc-jet conditions where the surface temperature reached ~2193 K for

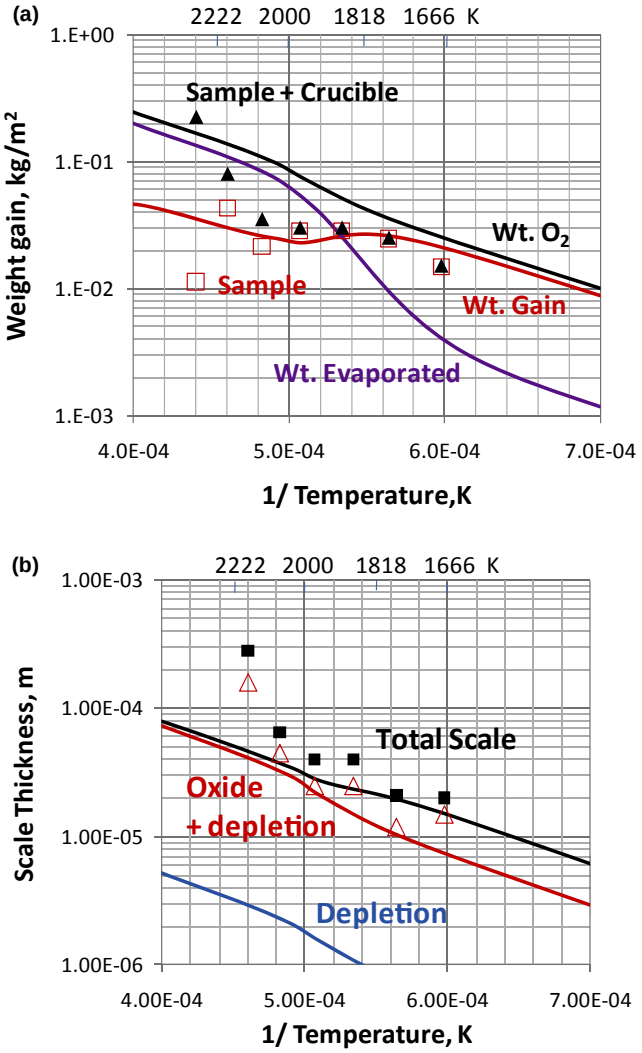

Fig. 6. Comparision of model with experimental data on oxidation kinetics of HfB_2–20 vol%SiC in the high-temperature regime (up to 2173 K) in static air showing weight gain in (a) and scale thicknesses in (b). All the data are from the work of Carney.[11] The solid lines are model predictions. In (a), both sample weight (open) and sample + crucible (filled) weights are shown, indicating flow is significant above 2000 K. Similarly in (b), total scale thickness (filled) and oxide scale thickness (open) are shown. Due to experimental ambiguity in demarcation between depletion and oxide scale, oxide scale + depletion thickness are shown for data and model.

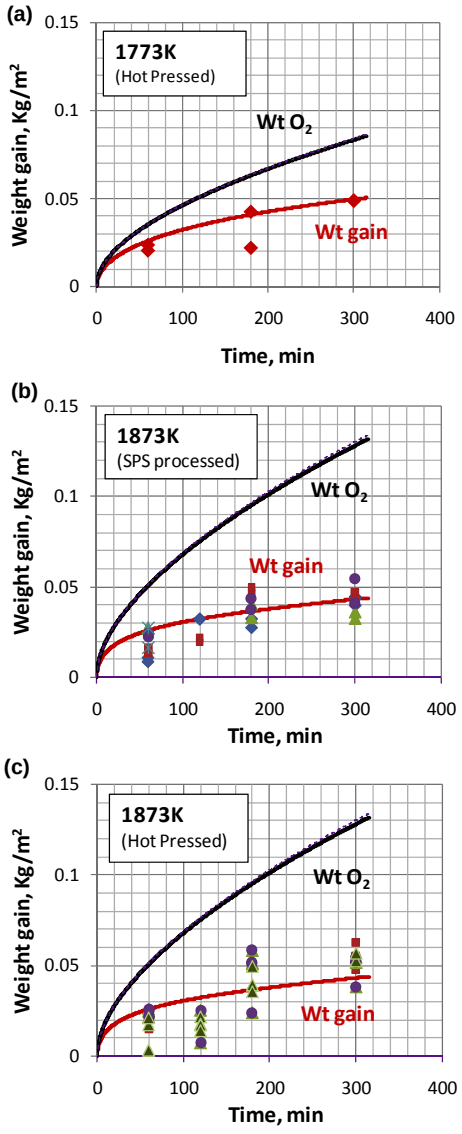

Fig. 7. Oxidation data on different batches of hot-pressed (a and c) and SPS-processed samples (b) of 20 vol%SiC–HfB_2 composition, collected at 1773 and 1873 K by Sevener.[20] The solid lines are model predictions for the weight gain and weight of oxygen consumed; the difference arises from evaporation of volatile oxides.

325 min.[55] From their metallographic images along with EDS maps, the thicknesses of the oxide layer, glass layer, and depletion layer were obtained. These are plotted along with model predictions in Fig. 8(a). A bilinear approximation of the measured temperature–time profile, used as input for the model, is shown as inset. More recently, Savino *et al.* have conducted a similar study at higher surface temperatures using the arc jet.[56] From the reported thermal history and calculated scale thicknesses from the published micrographs, the plot shown in Fig. 8(b) was generated which shows the model predictions compared to the data.

Data on arc jet tested samples of SiC–HfB_2 have been reported on by Carney[11] and Gasch *et al.*[12] In particular, Carney reported on scale thicknesses for both furnace-exposed and arc-jet-exposed samples of the same batch of sample under the same temperature (1773 K) and duration. Figure 8(c) shows the model predictions compared with furnace data and the arc-jet data. Figure 8(d) shows the data from Gasch *et al.*, who conducted two tests: one at surface temperature of 1803 K, and another at 1963 K. The model predictions for both these temperatures are shown.

In general, the model underpredicts the kinetics for experimental data on samples exposed to arc jet. The model is much closer at lower temperatures. The data from furnace-exposed samples show slower kinetics and are in reasonable correspondence with the model.

IV. Discussion

(1) Model Strength and Weaknesses

A model has been presented to interpret the oxidation kinetics of SiC-containing refractory metal diborides. The model includes the effect of viscous flow of the outer glassy scale and evaporative losses of volatile species under a boundary layer condition established by ambient fluid flow velocity. The model predicts the total weight of oxygen consumed, sample weight gain, weight of evaporated species, oxide thickness, glass thickness, depletion layer thickness, and recession of the substrate. The model uses as input parameters, the exposure temperature and time or a thermal profile, ambient oxygen partial pressure, gas chemistry, and fluid

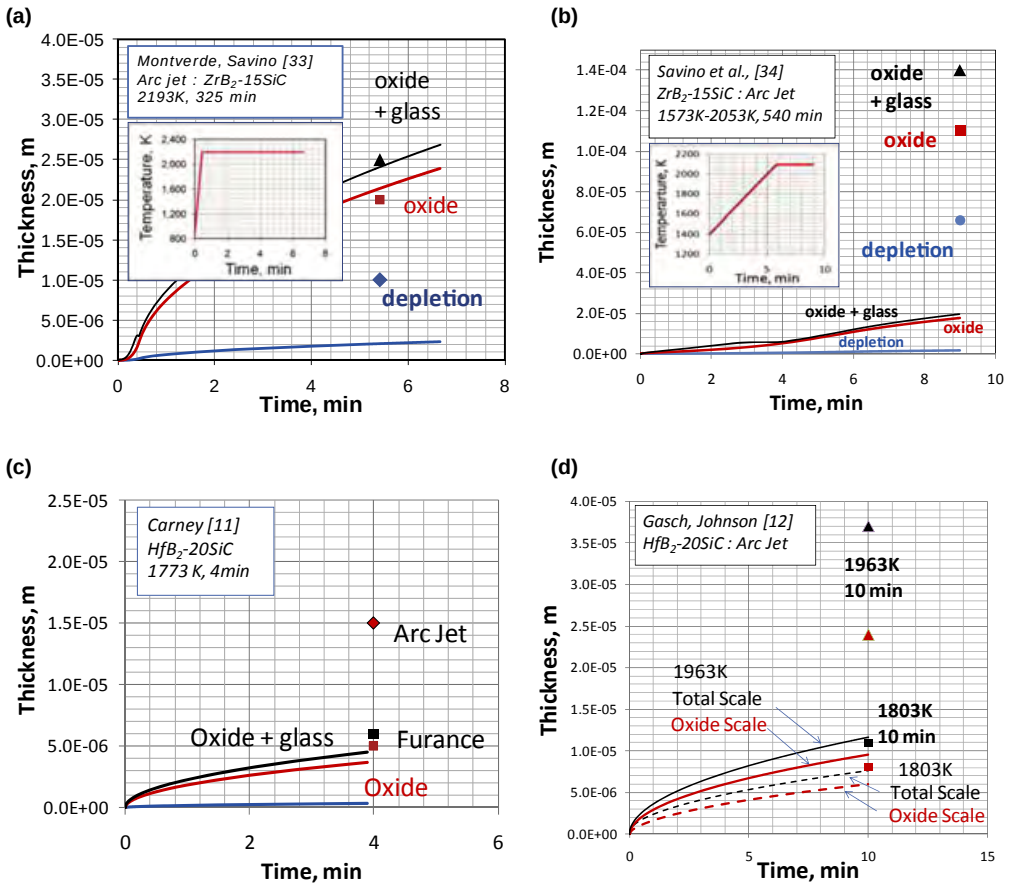

Fig. 8. Results from arc-jet testing done on ZrB_2–SiC (a and b) and on HfB_2–SiC (c and d) are shown along with model predictions for the reported thermal history used in the experiment (shown as inset in a and b) (data from ref. 11,12,55,56). In general, the model is seen to underpredict the oxidation kinetics, with the discrepancy increasing with temperature of exposure. In one case, shown in (c), a furnace oxidation and arc-jet run were conducted for the same temperature and time. The model is found to be much closer to the furnace-based data and well below the arc-jet data.

velocity. The material parameters for input are the size and volume fraction of SiC, sample length along the fluid flow direction. The model calculates the activity of boria in the oxide + glass region, but the activity of boria at the external glassy layer is assumed to be a fraction of the inner region. This was the only fit parameter. The model used a CO/CO_2 counter diffusion mechanism for oxygen transport within the depleted region.

In Fig. 2, the model is seen to be in agreement with the kinetics for oxidation of pure SiC in dry oxygen, although there is significant scatter in the data. This agreement shows that oxidation kinetics of SiC is limited by diffusion of molecular oxygen across the silica scale, assumed in the model. It further lends credibility to the assumption that the escape of CO, one of the oxidation products, is not rate limiting.

From Fig. 3, the effect of volume fraction of SiC on the kinetics of ZrB_2-based UHTCs is seen to be in agreement with the model for the two different sources of experimental data. The model predictions for the total oxygen consumed are shown by dotted lines, and the predicted sample weight gain by solid lines. The loss of material from the surface due to evaporation and fluid flow accounts for the difference between the two. Figure 3(c) confirms that the model captures the parabolic time dependence quantitatively.

In Fig. 4(a), the experimental data on weight gain agree well with the model, and the model predicts accelerated evaporation at temperatures above 1873 K. In Fig. 4(b), the measured scale thicknesses are in agreement with model within the bounds of scatter in the experimental data. The scatter arises from the variations in the flow of externally glassy layer, as detailed in Carney.[10] The data of Zhang *et al.*[14] were obtained using a zirconia furnace, where the possibility of contamination resulting in accelerated oxidation cannot be ruled out. The model predicts the depletion layer to be 2 μm at 1673 K rising to only 3 μm at 1873 K. Figure 5 shows that the evolution in time of weight gain and scale thicknesses agree well with the model. The data of Carney[10] at 1873 K and the data of Levine *et al.*[5] at 1600 and 1900 K are used to compare with the model. The two symbols for data of Carney refer to samples processed by SPS and hot pressing. The data of Levine *et al.* fall slightly below these. The depletion depths reported by Levine *et al.* at 1900 K are higher than the model prediction, while depletion was not observed by Carney at 1873 K.

The model predicts a finite but small depleted zone. The experimental reports show large variations. A 10-μm thick depletion zone was reported by Fahrenholtz at 1773 K in 30 min, whereas Zhang *et al.*[14] report no depleted zone below 1873 K. Similarly, no clear depleted zone was observed and reported by Carney after 2.5 h at 1673–1873 K. However, extensive EDS and FIB/TEM analyses did reveal a partially oxidized internal zone which was 2 μm at 1673 K and 14 μm at 1873 K. As the actual fraction of SiC oxidized in this partially oxidized zone was not measured, it is difficult to compare with this model. In summary, some ambiguity remains with respect to internal depleted zone formation in these materials.

In Fig. 6, the HfB_2–SiC data of Carney[11] are rationalized well by the model up to 2073 K, but there is a significant increase in measured oxidation compared to the predictions at 2173 K. The reasons for this remain unknown, but perhaps contamination from the stabilized zirconia heating elements may have caused this discrepancy because significant Ca was detected in EDS of the scales. The scales were found

to have a complex morphology at temperatures of 1973 K and above. The expected depletion layer was not observed; several different regions as detailed in Carney were noted.[11] Thus, the plot only shows the combined thickness of oxide and depletion layer, and the total scale thickness for the experimental data. Within experimental scatter, in Fig. 7, the model captures the evolution in time of weight gain at 1773 and 1873 K, as reported by Sevener.[20]

Figure 8 reveals the key inadequacy of the model. The oxidation kinetics during arc-jet testing were measured and reported by Montverde and Savino for ZrB_2–15SiC under two different heat flux conditions.[55,56] The actual thermal profiles reported were used in the model. The model fails to capture even the correct order of magnitude of scale thicknesses at high heat fluxes, while it is reasonable for low heat flux conditions. The internal depletion is considerably underpredicted. Similarly for HfB_2–20SiC, the model underpredicts the kinetics by a significant margin. In one reported work, both furnace oxidation and arc-jet oxidation were conducted at the same temperature and time, viz. 1773 K for 4 min. Figure 8(d) shows that once again, the model captures arc-jet data better at lower temperatures, but not at higher temperatures using data from Gasch *et al.* on HfB_2–20SiC.[12] The model prediction is close for the furnace oxidation data, but far below the arc-jet data. Clearly, aspects of oxidation kinetics that take place during arc-jet conditions are not captured in the model.

(2) Future Directions

The model is clearly lacking in capturing high-temperature oxidation kinetics under arc-jet conditions. Several possible mechanisms can be suggested that require further analysis and experimentation. The dissociation of gases into monatomic oxygen and nitrogen under arc-jet conditions is well-known.(for example, see ref. 57) However, the oxidation mechanisms under such conditions have only been studied by a few.[58,59] These studies show that oxidation is indeed faster under dissociated oxygen conditions; however, the reasons for this have not been established. The recombination of the monatomic gases at the material surface can release energy that is sufficient to raise the material surface temperature. In the furnace oxidation tests using monatomic oxygen, the material surface temperature could not be measured. However, during arc-jet testing, the material temperature was measured, and the model is unable to capture the oxidation kinetics with these measured temperatures, indicating that some other mechanism might play a role. The possibility of enhanced oxidation kinetics from permeation of oxygen in monatomic form has been suggested, but no direct experimental evidence exists. A modeling work by Li *et al.* based on first principles showed that the dissolved concentration of monatomic oxygen in borosilicate glasses can be higher than that of diatomic oxygen, at temperatures above 1773 K.[60] Given that the arc-jet test data are closer to the model at lower temperatures (below 1900 K) and deviate significantly at higher temperatures, the enhanced permeation by monatomic oxygen in borosilicate glasses at higher temperatures is a possibility. Monatomic oxygen would also change the thermodynamics of oxidation at the ZrB_2/oxide interface. Theoretical and experimental investigations that could confirm this hypothesis are suggested for future work. It is also suggested that the possibility of active oxidation of SiC from the surface by monatomic oxygen be investigated. The effect of mechanical shear at high velocities has been neglected in this work; however, the model predicts evaporation to be high enough to predict the absence of external glass under arc-jet conditions.

Another limitation of the model is its inability to predict the depletion layer thicknesses in all the reported works. However, there is considerable disagreement between different works on the extent and even existence of the depletion layer under identical conditions for similar or identical compositions. The model shows clearly that counter diffusion via the CO/CO_2 mixture as oxygen transport medium is tenable and can lead to a depleted region. However, the extent is not as high as in some of the reports, while it is consistent with others. Some uncontrolled variable, such as humidity or sample porosity, within the experiment might be responsible for this. Future studies that clarify this might be useful. Finally, the effect of mechanical forces that induce shear of the external glass by viscous flow has been ignored in this work and may be worth examining in future models.

V. Summary

A mechanistic model has been built to interpret experimental data on the oxidation kinetics of SiC-containing diborides of Zr and Hf in the temperature regime of 1473–2473 K. The model uses available viscosity, thermodynamic and kinetic data on borosilicate glasses, and uses a logarithmic mean approximation for compositional variations. The internal depletion region of SiC is modeled using counter diffusion in CO/CO_2 as oxygen transport mechanism. Data obtained after furnace oxidation of pure SiC in oxygen, SiC-containing ZrB_2 with varying volume fractions, and SiC–HfB_2 UHTCs were found to agree reasonably well with the model. The model predictions include weight of oxygen consumed, sample weight gain, external glassy layer thickness, inner oxide scale thickness, recession, and depletion layer thickness. Some depletion layer thicknesses and data obtained using arc-jet tests fall well outside the model predictions, indicating that some aspects of arc-jet conditions are not captured in this model.

Acknowledgments

We acknowledge useful discussions with Dr. I. Talmy of NSWC, MD. It is also a pleasure to acknowledge several useful suggestions made by Prof. E. Opila of Univ. of Virgina, during manuscript preparation.

References

[1]M. M. Opeka, I. G. Talmy, and J. A. Zaykoski, "Oxidation-Based Materials Selection for 2000°C+ Hypersonic Aerosurfaces: Theoretical Considerations and Historical Experience," *J. Mater. Sci.*, **39**, 5887–904 (2004).

[2]M. M. Opeka, I. G. Talmy, E. J. Wuchina, J. A. Zaykoski, and S. J. Causey, "Mechanical, Thermal and Oxidation Properties Of Refractory Hafnium and Zirconium Compounds," *J. Eur. Ceram. Soc.*, **19**, 2405–14 (1999).

[3]E. Wuchina, M. Opeka, S. Causey, K. Buesking, J. Spain, A. Cull, J. Routbort, and F. Guitierrez-Mora, "Designing for Ultrahigh-Temperature Applications: The Mechanical and Thermal Properties of HfB2, HfCx, HfNx and a-Hf(N)," *J. Mater. Sci.*, **39**, 5939–49 (2004).

[4]E. Opila, S. Levine, and J. Lorincz, "Oxidation of ZrB2 and HfB2-Based Ultra-High Temperature Ceramics: Effect of Ta Additions," *J. Mater. Sci.*, **39** [19] 5969–77 (2004).

[5]S. R. Levine, E. J. Opila, M. C. Halbig, J. D. Kiser, M. Singh, and J. A. Salem, "Evaluation of Ultra-High Temperature Ceramics for Aeropropulsion Use," *J. Eur. Ceram. Soc.*, **22**, 2757–67 (2002).

[6]F. Monteverde, "Progress in the Fabrication of Ultra-High-Temperature Ceramics: "In Situ" Synthesis, Microstructure and Properties of a Reactive Hot-Pressed HfB2–SiC Composite," *Comp. Sci. Tech.*, **65**, 1869–79 (2005).

[7]W. G. Fahrenholtz, "Thermodynamic Analysis of ZrB2–SiC Oxidation: Formation of a SiC-Depleted Region," *J. Am. Ceram. Soc.*, **90** [1] 143–8 (2007).

[8]A. Rezaie, W. G. Fahrenholtz, and G. E. Hilmas, "Evolution of Structure During the Oxidation of Zirconium Diboride–Silicon Carbide in Air up to 1500 °C," *J. Eur. Ceram. Soc.*, **27**, 2495–501 (2007).

[9]F. Monteverde, "The Thermal Stability in Air of Hot-Pressed Diboride Matrix Composites for Uses at Ultra-High Temperatures," *Corros. Sci.*, **47**, 2020–33 (2005).

[10]C. M. Carney, P. Mogilevsky, and T. A. Parthasarathy, "Oxidation Behavior of Zirconium Diboride Silicon Carbide Produced by the Spark Plasma Sintering Method," *J. Am. Ceram. Soc.*, **92** [9] 2046–52 (2009).

[11]C. M. Carney, "Oxidation Resistance of Hafnium Diboride-Silicon Carbide from 1400-2000C," *J. Mater. Sci.*, **44**, 5673–81 (2009).

[12]M. Gasch and S. Johnson, "Physical Characterization and Arcjet Oxidation of Hafnium-Based Ultra High Temperature Ceramics Fabricated by Hot Pressing and Field-Assisted Sintering," *J. Eur. Ceram. Soc.*, **30**, 2337–44 (2010).

[13]E. J. Opila and M. C. Halbig, "Oxidation of ZrB2-SiC," *Ceram. Eng. Sci. Proc.*, **22** [3] 221–8 (2001).

[14]X.-H. Zhang, P. Hu, and J.-C. Han, "Structure Evolution of ZrB2-SiC During the Oxidation in Air," *J. Mater. Res.*, **23** [7] 1961–72 (2008).

[15]M. Wang, C.-A. Wang, L. Yu, Y. Huang, and Z. Zhang, "Oxidation Behavior of SiC Platelet-Reinforced ZrB2 Ceramic Matrix Composites," *Int. J. Appl. Ceram. Tech.*, (2011). doi: 10.1111/j.1744-7402.2011.02647.x.

[16]W.-B. Han, P. Hu, X.-H. Zhang, J.-C. Han, and S.-H. Meng, "High-Temperature Oxidation at 19001C of ZrB2–xSiC Ultrahigh-Temperature Ceramic Composites," *J. Am. Ceram. Soc.*, **91** [10] 3328–34 (2008).

[17]S. N. Karlsdottir and J. W. Halloran, "Formation of Oxide Scales on Zirconium Diboride–Silicon Carbide Composites During Oxidation: Relation of Subscale Recession to Liquid Oxide Flow," *J. Am. Ceram. Soc.*, **91** [11] 3652–8 (2008).

[18]S. N. Karlsdottir and J. W. Halloran, "Oxidation of ZrB2-SiC: Influence of SiC Content on Solid and Liquid Oxide Phase Formation," *J. Am. Ceram. Soc.*, **92** [2] 481–6 (2009).

[19]S. Gangireddy, S. N. Karlsdottir, and J. W. Halloran, "High-Temperature Oxidation at 19001C of ZrB2–xSiC Ultrahigh-Temperature Ceramic Composites," *Key Eng. Mater.*, **434–435**, 144–8 (2010).

[20]K. Sevener, *Oxidation of HfB2-SiC Ultra-High Temperature Ceramics at 1500°C - 1600°C*. US Air Force Summer Faculty Fellowship, Wright-Patterson AFB, OH, 2007.

[21]E. Opila, S. Levine, and J. Lorincz, "Oxidation of ZrB2- and HfB2-Based Ultra-High Temperature Ceramics: Effect of Ta Additions," *J. Mater. Sci.*, **39**, 5969–77 (2004).

[22]T. A. Parthasarathy, R. A. Rapp, M. Opeka, and R. J. Kerans, "A Model for the Oxidaiton of ZrB2, HfB2 and TiB2," *Acta Mater.*, **55**, 5999–6010 (2007).

[23]T. A. Parthasarathy, R. A. Rapp, M. Opeka, and R. J. Kerans, "A Model for Transitions in Oxidation Regimes of ZrB2," *Mater. Sci. Forum*, **595–598**, 823–32 (2008).

[24]T. A. Parthasarathy, R. A. Rapp, M. Opeka, and R. J. Kerans, "Effect of Phase Change and Oxygen Permeability in Oxide Scales on Oxidation Kinetics of ZrB2 and HfB2," *J Am. Ceram. Soc.*, **92** [5] 1079–86 (2009).

[25]F. Monteverde and A. Bellosi, "Oxidation of ZrB2-Based Ceramics in Dry Air," *J. Electrochem. Soc.*, **150** [11] B552–9 (2003).

[26]G. R. Holcomb and G. R. St.Pierre, "Application of a Counter-Current Gaseous Diffusion Model to the Oxidation of Hafnium Carbide at 1200C to 153OC," *Oxid. Met.*, **40** [1/2] 109–18 (1993).

[27]K. L. Luthra, "Some New Perspectives on Oxidation of Silicon Carbide and Silicon Nitride," *J. Am. Ceram. Soc.*, **74**, 1095–103 (1991).

[28]M. Boike, K. Hilpert, and F. Muller, "Thermodynamic Activities in B_2O_3-SiO_2 Melts at 1475 K," *J. Am. Ceram. Soc.*, **76** [11] 2809–12 (1993).

[29]Y. Kawamoto, T. Horisaka, and M. Tomozawa, "Absence of Phase Separation in the System Boron Oxide-Silica," *Glastech. Ber.*, **56**, 782–7 (1983).

[30]W. M. Kays and M. E. Crawford, *Convective Heat and Mass Transfer*. 2nd edition, p. 139, McGraw-Hill, New York, 1980.

[31]R. H. Perry and C. H. Chilton, *Chemical Engineers' Handbook*. McGraw-Hill Book Company, New York, NY, 1973.

[32]I. Barin, *Thermochemical Data of Pure Substances I*. in 3rd edition ed.). VCH Verlagsgesellschaft, New York, 1995.

[33]R. A. Svehla, "Estimated Viscosities and Thermal Conductivities of Gases at High Temperatures"; in NASA Tech report R-132, Washington DC, 1962.

[34]T. Kawamoto, T. Horisaka, and M. Tomozawa, "Absence of Phase Separation in the System Boron Oxide-Silica," *Glastch. Ber.*, **56**, 782–7 (1980).

[35]R. A. Eppler, "Viscosity of Molten B_2O_3," *J. Am. Ceram. Soc.*, **49** [12] 679–80 (1966).

[36]P.-C. Li, A. C. Ghose, and G.-J. Su, "Viscosity Determination of Boron Oxide and Binary Borates," *J. Am. Ceram. Soc.*, **45** [2] 83–8 (1962).

[37]R. H. Doremus, "Viscosity of Silica," *J. Appl. Phys.*, **92** [12] 7619–29 (2002).

[38]G. Urbain, Y. Bottinga, and P. Richet, "Viscosity of Liquid Silica, Silicates and Alumino-silicates," *Geochim. Cosmochim. Acta*, **46**, 1061 (1982).

[39]G. Hetherington, K. H. Jack, and J. C. Kennedy, "The Viscosity of Vitreous Silica," *Phys. Chem. Glasses*, **5**, 130 (1964).

[40]A. Fluegel, "Glass Viscosity Calculation Based on a Global Statistical Modelling Approach," *Eur. J. Glass Sci. Tech., A*, **48** [1] 13–30 (2007).

[41]P. Hrma, B. M. Arrigoni, and M. J. Schweiger, "Viscosity of Many-Component Glasses," *J. Non-Cryst. Solids*, **355**, 891–902 (2009).

[42]T. Tokuda, T. Ido, and T. Yamaguchi, *Z Natuforschung*, **26A**, 2058–60 (1971).

[43]K. L. Luthra, "Oxidation of Carbon/Carbon Composites – A Theoretical Analysis," *Carbon*, **26**, 217–24 (1988).

[44]J. Schlichting, "Oxygen Transport Through Glass Layers Formed by a Gel Process," *J. Non-Cryst. Solids*, **63**, 173–81 (1984).

[45]M. A. Lamkin, F. L. Riley, and R. J. Fordham, "Oxygen Mobility in Silicon Dioxide and Silicate Glassses: A Review," *J. Eur. Ceram. Soc.*, **10**, 347–67 (1992).

[46]E. L. Courtright, "Engineering Property Limitations of Structural Ceramics and Ceramic Composites Above 1600C," *Ceram. Eng. Sci. Proc.*, **12** [9–10] 1725–44 (1991).

[47]C. E. Ramberg and W. L. Worrell, "Oxygen Transport in Silica at High Temperatures: Implications of Oxidation Kinetics," *J. Am. Ceram. Soc.*, **84** [11] 2607–16 (2001).

[48]C. E. Ramberg, G. Cruciani, K. E. Spear, R. E. Tressler, and C. F. Ramberg, "Passive-Oxidation Kinetics of High-Purity Silicon Carbide from 800 to 1100 C," *J. Am. Ceram. Soc.*, **79** [11] 2897–911 (1996).

[49]J. A. Costello and R. A. Tressler, "Oxidation Kinetics of Silicon Carbide Crystals and Ceramics: I. In Dry Oxygen," *J. Am. Ceram. Soc.*, **69** [9] 674–81 (1986).

[50]P. Mogilevsky, E. E. Boakye, R. S. Hay, J. Welter, and R. J. Kerans, "Monazite Coatings on SiC Fibers II: Oxidation Protection," *J. Am. Ceram. Soc.*, **89** [11] 3481–90 (2006).

[51]Z. Zheng, R. E. Tressler, and K. E. Spear, "Oxidation of Single Crystal Silicon Carbide," *J. Electrochem. Soc.*, **137**, 854–8 (1990).

[52]R. C. A. Harris, "Oxidation of 6h Alpha Silicon Carbide Platelets," *J. Am. Ceram. Soc.*, **58**, 7–9 (1975).

[53]L. U. J. T. Ogbuji and E. J. Opila, "A Comparison of the Oxidation Kinetics of SiC and Si3N4," *J. Electrochem. Soc.*, **142**, 925–30 (1995).

[54]I. Talmy, *Effect of SiC Content on Oxidation Kinetics of SiC-ZrB2*. Unpublished work, Naval Surface Warfare Center, Carderock, MD, 2005.

[55]F. Montverde and R. Savino, "Stability of Ultra-High-Temperature ZrB2–SiC Ceramics Under Simulated Atmospheric Re-Entry Conditions," *J. Eur. Ceram. Soc.*, **27**, 4797–805 (2007).

[56]R. Savino, M. D. S. Fumo, D. Paterna, A. D. Maso, and F. Monteverde, "Arc-Jet Testing of Ultra-High-Temperature-Ceramics," *Aerospace Sci. Technol.*, **14**, 178–87 (2010).

[57]J. Marschall and D. G. Fletcher, "High-Enthalpy Test Environments, Flow Modeling and In Situ Diagnostics for Characterizing Ultra-High Temperature Ceramics," *J. Eur. Ceram. Soc.*, **30**, 2323–36 (2010).

[58]B. R. Rogers, Z. Song, J. Marschall, N. Queralto, and C. A. Zorman, "The Effect of Dissociated Oxygen on the Oxidation of Si, Polycrystalline SiC and LPCVD Si3N4," *High Temp. Corr. Mater. Chem.*, **PV 2004-16**, 268–78 (2004).

[59]J. Marschall, D. A. Pejakovic, W. G. Fahrenholtz, G. E. Hilmas, S. Zhu, J. Ridge, D. G. Fletcher, C. O. Asma, and J. Thomel, "Oxidation of ZrB2–SiC Ultrahigh-Temperature Ceramic Composites in Dissociated Air," *J. Thermophys. Heat Transfer*, **23** [2] 267–78 (2009).

[60]J. Li, T. J. Lenosky, C. J. Forst, and S. Yip, "Thermochemical and Mechanical Stabilities of the Oxide Scale of ZrB2 + SiC and Oxygen Transport Mechanisms," *J. Am. Ceram.Soc.*, **91** [5] 1475–80 (2008). □